Supporting information

Anomalous Dominated (100) Index Facet Endows Ruthenium Nanoparticles Accelerating Alkaline Hydrogen Evolution

Xuemei Cui[1], Zijian Li[2], Haeseong Jang[3], Min Gyu Kim[4], Shangguo Liu[1,], Liqiang Hou[1,*], Xien Liu[1,*]*

[1]College of Chemical Engineering, Qingdao University of Science and Technology, Qingdao 266042, P. R. China

[2]Department of Chemistry, City University of Hong Kong, Hong Kong, SAR 999077, P. R. China

[3]Department of Advanced Materials Engineering, Chung-Ang University, Seoul 156-756, South Korea

[4]Beamline Research Division, Pohang Accelerator Laboratory (PAL), Pohang 37673 (Korea)

[*]E-mail addresses: S. Liu, liusg@qust.edu.cn; L. Hou, houliqiang@qust.edu.cn; X. Liu, liuxien@qust.edu.cn

This file contains:

Details of experimental sections

Number of pages: 22

Number of Figures: 14

Number of Tables: 2

Experimental Sections

Synthesis of samples

ZIF-67 was prepared as follows: an 80 mL methyl alcohol solution containing $Co(NO_3)_2 \cdot 6H_2O$ (3.287 g) was rapidly injected into 120 mL of methyl alcohol solution containing 2-methylimidazole (8 g). Then, the mixed solution was stirred at room temperature for 6 h. The ZIF-67 were collected via several centrifugation-washing three cycles by methyl alcohol and dried at 60 °C.

The substitute with phytic acid (PA) was as follows: First, 50 mg of ZIF-67 and 100 mg of PVP were dispersed into 50 mL of ethanol and stirred at room temperature to form mixed solution A. Then, 5 mL of an ethanol solution of phytic acid (V_{PA}: $V_{ethanol}$ = 1:40) was dropwise added to the mixed solution A. After this, the solution was stirred at room temperature for 60 min. Finally, the product was washed with ethanol several times and dried at 60 °C. The obtained product was named Co-PA.

The substitute with ruthenium ions ($RuCl_3 \cdot xH_2O$) was as follows: First, 10 mg of Co-PA were dispersed into 10 mL of deionized water through the ultrasonic treatment for 10 min. Then, 3 mg $RuCl_3 \cdot xH_2O$ was added to the above solution and stirred at room temperature for 24 h. The product was collected via suction filtration and dried at 60 °C. The obtained product was named Ru-PA.

Ru(100)/NPC was prepared as follows: the Ru-PA was annealed at 650 °C for 2 h under the H_2/Ar atmosphere. After cooling to room temperature, the obtained product was named Ru(100)/NPC.

For comparison, 10 mg of ZIF-67 were dispersed into 10 mL of deionized water through the ultrasonic treatment for 10 min. Then, 3 mg $RuCl_3 \cdot xH_2O$ was added to the above solution and stirred at room temperature for 48 h. The product was collected via suction filtration and dried at 60 °C. The obtained product was named Ru-MOF. Finally, the Ru-MOF was annealed at 650 °C for 2 h under the H_2/Ar atmosphere. After cooling to room temperature, the obtained product was named Ru(101)/NC.

Materials Characterizations

The crystallographic structure of the samples was investigated by X-ray diffraction (XRD, DX2700, China) operating with Cu Kα radiation (l=1.5418 Å) with an accelerating voltage of 40 kV. Transmission electron microscopy (TEM) and elemental mapping were performed on a jeol2100F transmission electron microscope at an accelerating voltage of 120 kV. An inductively coupled plasma-optical emission spectrophotometer (ICP-OES, 700-ES, Varian) was used to detect the Ru content in the composite. X-ray photoelectron spectroscopy (XPS) of the catalysts was obtained by ESCALab250 electron spectrometer (Thermo Scientific Corporation) with mono-chromatic 150 W Al Kα radiation. X-ray absorption near-edge structure (XANES) and extended X-ray absorption fine structure (EXAFS) were performed using a BL10C beam line (Wide energy EXAFS) with a Pohang light source-II (PLS-II) in top-up mode operation under a ring current of 300 mA at 3.0 GeV. The texture coefficients (T($h_ik_il_i$)) of the (100) and (101) in Ru(100)/NPC and Ru(101)/NC were confirmed by the following relationship: T($h_ik_il_i$) = I/I_0/($1/n\{\Sigma(I/I_0)\}$), in which i=1,2,3….n, I is the relative diffraction intensity for ($h_ik_il_i$) plane of the sample under investigation, I_0 is the relative intensity for ($h_ik_il_i$) plane of the standard profile from JCPDS, and n is the number of reflections.

The calculation details for (100) and (101) were given as follows:

For (100) and (101) facet of Ru(100)/NPC:

$$T_{(100)} = \frac{I(100)/I_0(100)}{1/n\left\{\sum\left(I(hikili)/I_0(hikili)\right)\right\}} = \frac{4958/40}{\frac{1}{6}\left(\frac{4928}{40}+\frac{1611}{35}+\frac{3196}{100}+\frac{665}{25}+\frac{937}{25}+\frac{765}{25}\right)} = 2.5$$

$$T_{(101)} = \frac{I(101)/I_0(101)}{1/n\left\{\sum\left(I(hikili)/I_0(hikili)\right)\right\}} = \frac{\frac{3196}{100}}{\frac{1}{6}\left(\frac{4928}{40}+\frac{1611}{35}+\frac{3196}{100}+\frac{665}{25}+\frac{937}{25}+\frac{765}{25}\right)} = 0.65$$

For (100) and (101) facet of Ru(101)/NC:

$$T_{(100)} = \frac{I(100)/I_0(100)}{1/n\left\{\sum\left(I(hikili)/I_0(hikili)\right)\right\}} = \frac{51/40}{\frac{1}{6}\left(\frac{51}{40}+\frac{49.5}{35}+\frac{123}{100}+\frac{27}{25}+\frac{25}{25}+\frac{23}{25}\right)} = 1.1$$

$$T_{(101)} = \frac{I(101)/I_0(101)}{1/n\left\{\sum\left(I(hikili)/I_0(hikili)\right)\right\}} = \frac{123/100}{\frac{1}{6}\left(\frac{51}{40}+\frac{49.5}{35}+\frac{123}{100}+\frac{27}{25}+\frac{25}{25}+\frac{23}{25}\right)} = 1.1$$

Electrochemical measurements

For the preparation of the working electrode, 2 mg catalyst was dispersed in the mixture of 40 μL of Nafion (5 wt. %) solution and 300 μL of ethanol. Then a homogenous catalyst ink was obtained by an ultrasonic disperse method. 5 μL of the ink was pipetted onto a glassy carbon disk (0.07065 cm^2). The electrochemical experiments were carried out at room temperature using CHI 760E workstation with a standard three-electrode system, where a Hg/HgO and a carbon rod as the reference and counter electrode, respectively. The LSVs for HER were recorded at the potential range from -0.05 to 0.3 V vs. RHE in 1.0 M KOH. To obtain fully consistent LSVs, all the samples require repetitive potential scans. The electrochemically active surface area (ECSA) of the electrocatalyst is estimated from the double-layer capacitance (C_{dl}). CV curves involving in the H_{upd} adsorption/desorption peak were obtained in an Ar-saturated 1.0 M KOH solution with potential window between 0 V and 1.0 V vs. RHE and a sweep rate of 20 mV s^{-1}. All the LSVs are compensated by 95% iR-drop. The potentials were converted to the RHE potential by using $E_{RHE} = E_{Hg/HgO} + 0.0977 + 0.059 \times pH$.

DFT Calculations

All density functional theory calculations in this study are performed by using the Vienna ab initio simulation package (VASP).[1] The Perdew-Burke-Ernzerhof (PBE)[2] functional is employed to treat the exchange-correlation interactions. The plane-wave basis set with a kinetic energy cutoff of 400 eV, the energy convergence criterion of 10^{-5} eV, the force convergence criterion of 0.02 eV $Å^{-1}$, and a (1×1×1) Monkhorst-Pack k-point sampling is employed for structure relaxation. For different surface models, the bottom layer is fixed. A sufficiently large vacuum gap (> 15 Å) is employed to prevent the interaction between neighboring periodic structures along the c axis. H_2 and H_2O were calculated in boxes of 20 Å×20 Å×20 Å with the gamma point only. The CI-NEB method was adopted to search the minimum energy paths of H_2O dissociation reaction [3,4]. Six images are used for CI-NEB

calculations. The free energy diagrams for HER are calculated with reference to the computational hydrogen electrode.[5] The free energy of the gas phase and adsorbed species can be obtained from the following equation:

$$\Delta G = \Delta E_{DFT} + \Delta ZPE - T\Delta S$$

where E_{DFT} is the electronic energy, and T was set as 298.15 K. ΔZPE and TΔS are the change in the zero point energy and entropy at room temperature (T=298.15 K), which are obtained after frequency calculations.

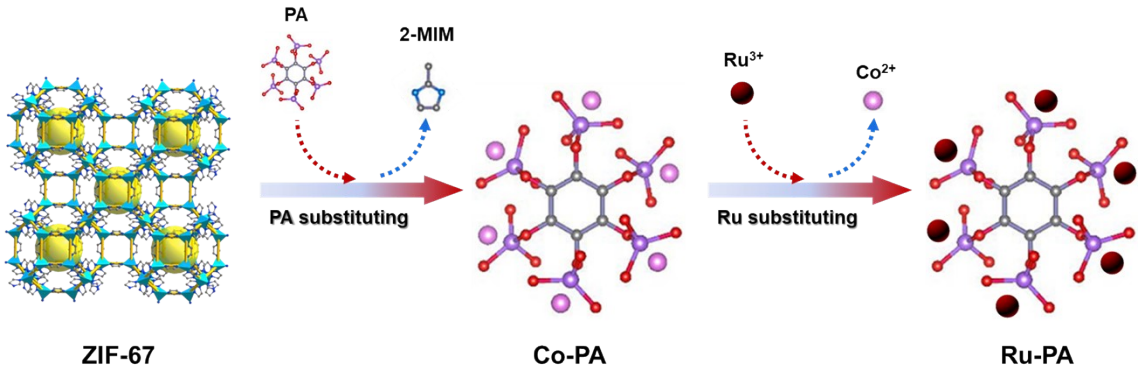

Fig. S1. Illustration of gradual substitute method.

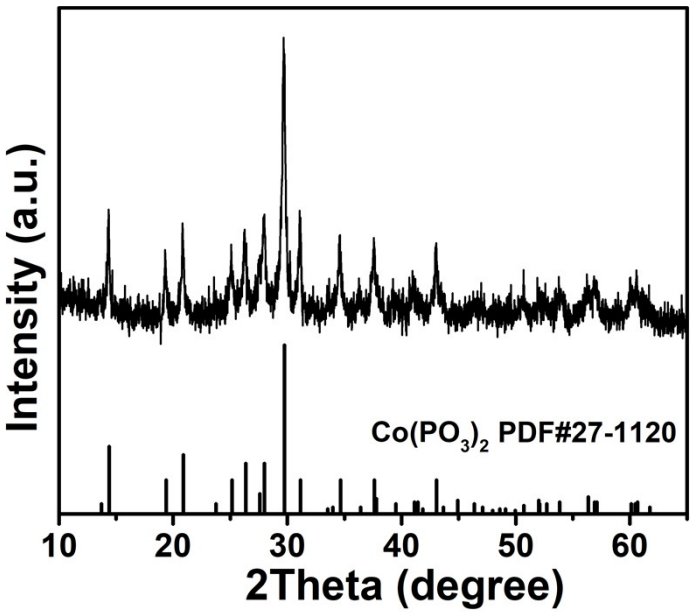

Fig. S2. XRD pattern of the obtained product from the individually substituted by PA.

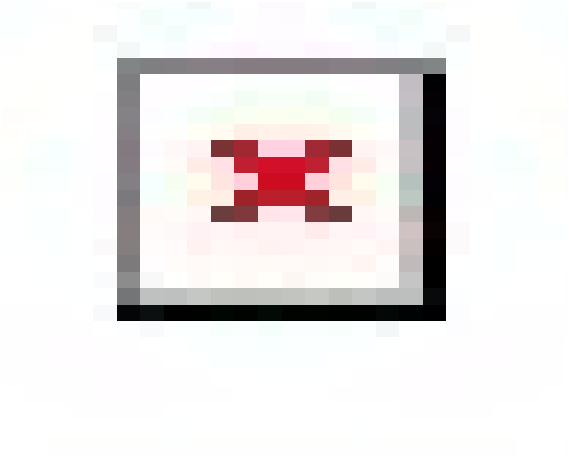

Fig. S3. XRD pattern of the obtained product from the individually substituted by Ru^{3+}.

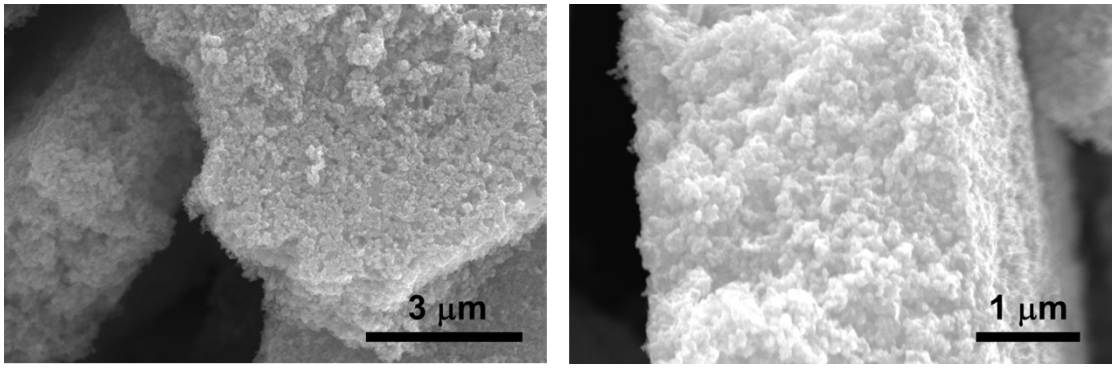

Fig. S4. The SEM images of Ru(100)/NPC.

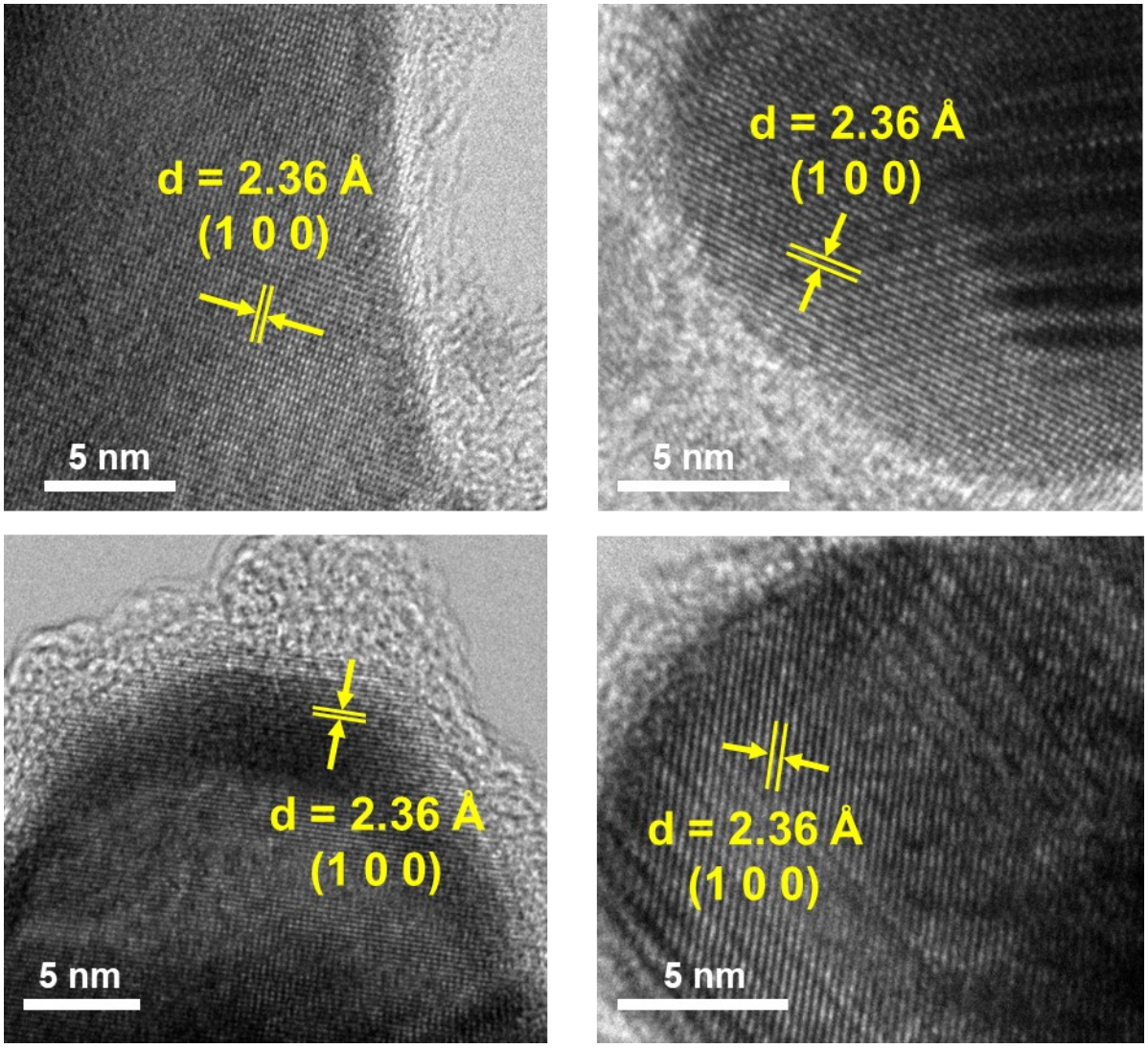

Fig. S5. TEM images of Ru(100)/NPC.

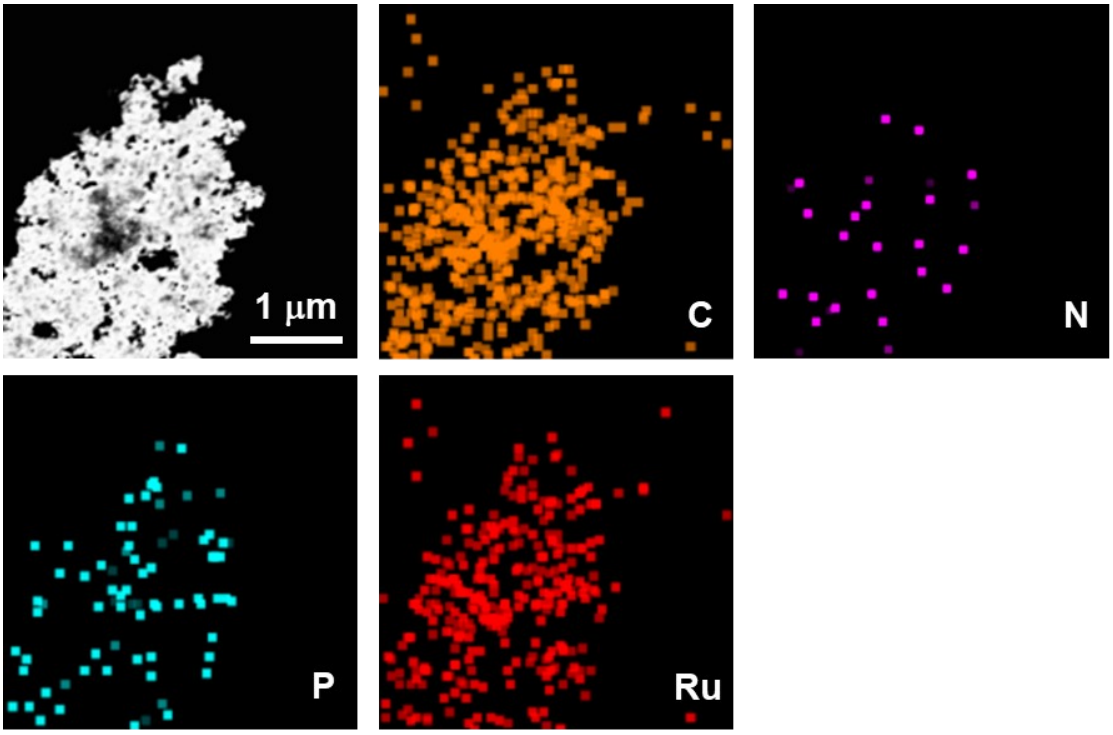

Fig. S6. The EDS elemental mapping of Ru(100)/NPC.

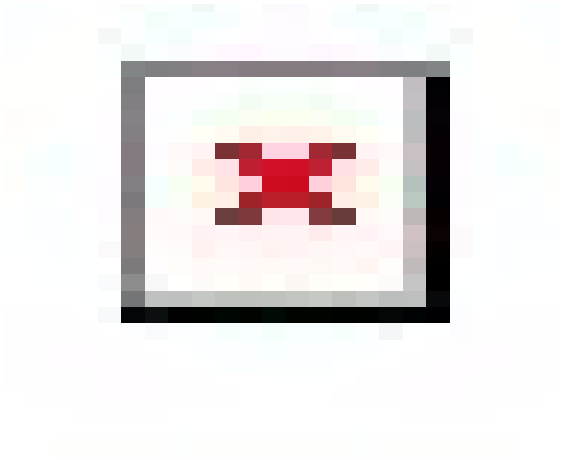

Fig. S7. Ru3p XPS spectrum of air-exposed Ru metal.

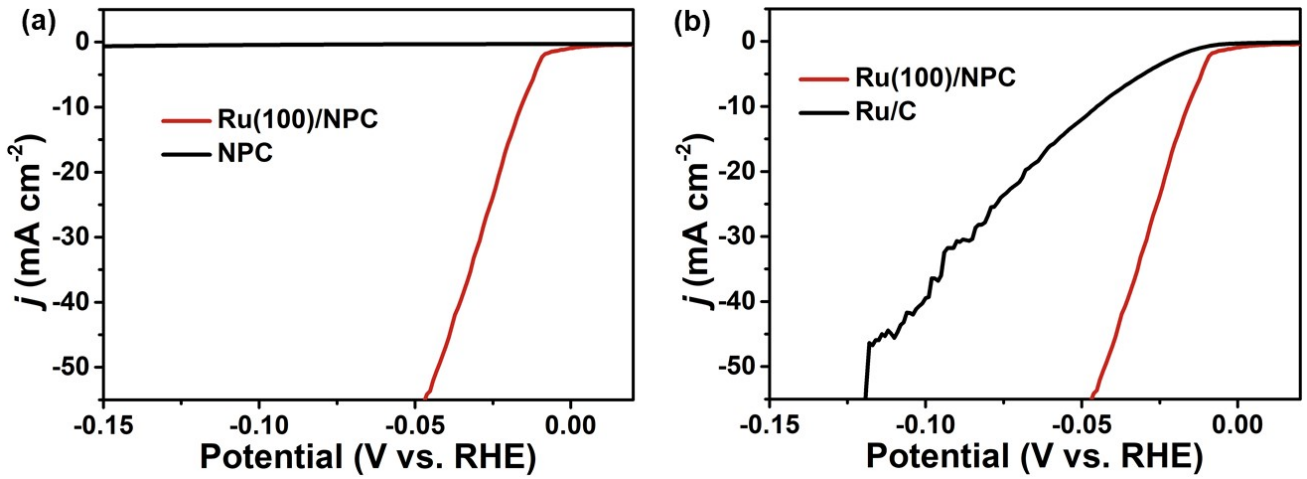

Fig. S8. (a) Polarization curves of Ru(100)/NPC and NPC in an Ar-saturated 1 M KOH solution with a scan rate of 5 mV s^{-1}. (b) Polarization curves of Ru(100)/NPC and commercial Ru/C in an Ar-saturated 1 M KOH solution with a scan rate of 5 mV s^{-1}.

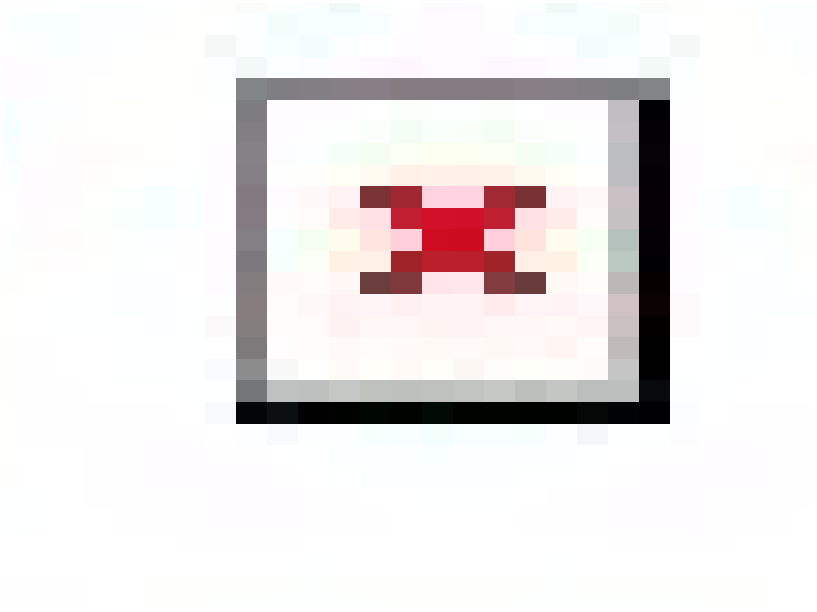

Fig. S9. Exchange current density of Ru(100)/NPC, Ru(101)/NC, and Pt/C.

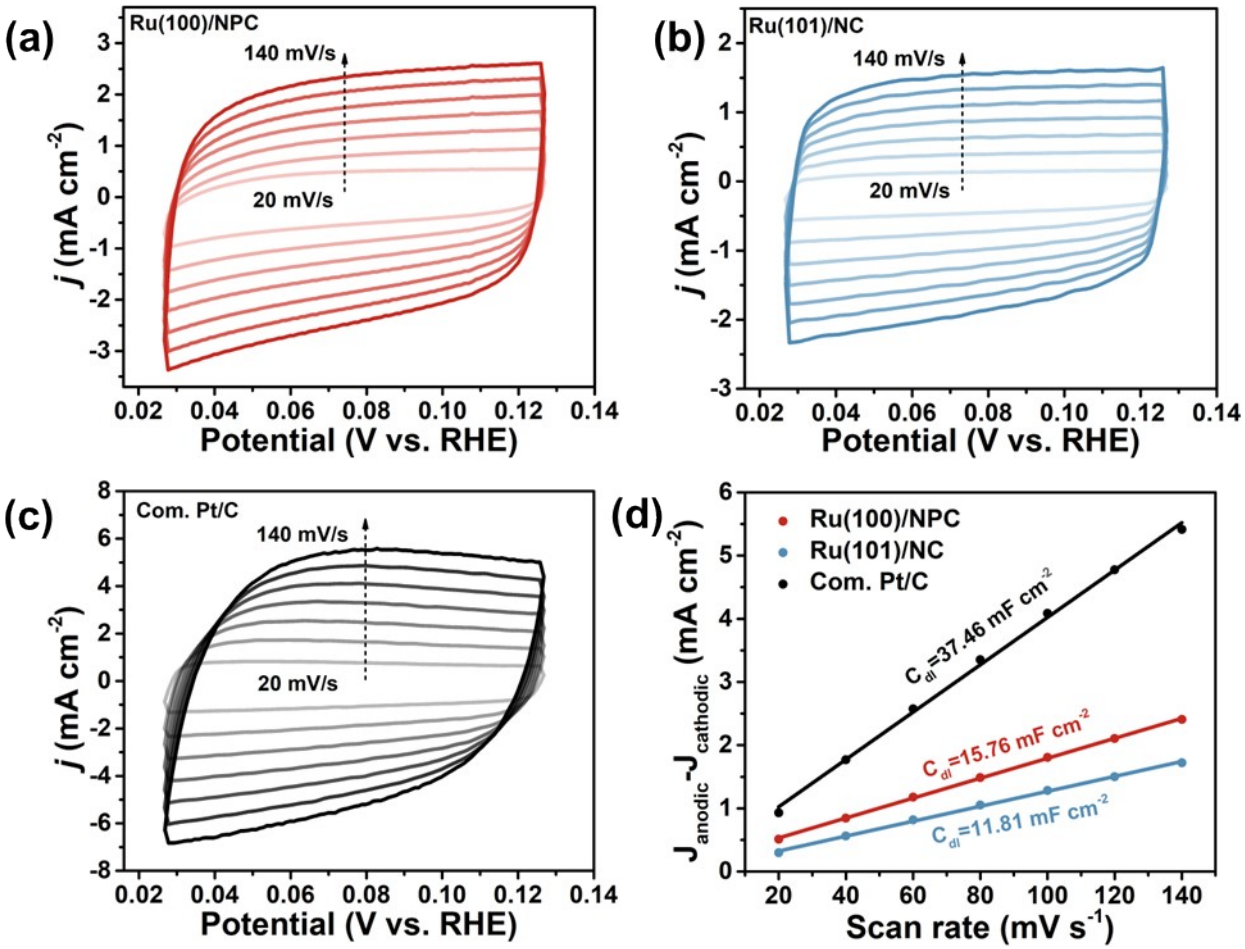

Fig. S10. The ECSA of Ru(100)/NPC, Ru(101)/NC, and Com. Pt/C are obtained as 27.84, 20.86, and 66.16 cm^2, respectively, following the equation ECSA = $(C_{dl}*A)/C_s$ (A is the area of working electrode; C_s = 0.04 mF cm^{-2}).[6]

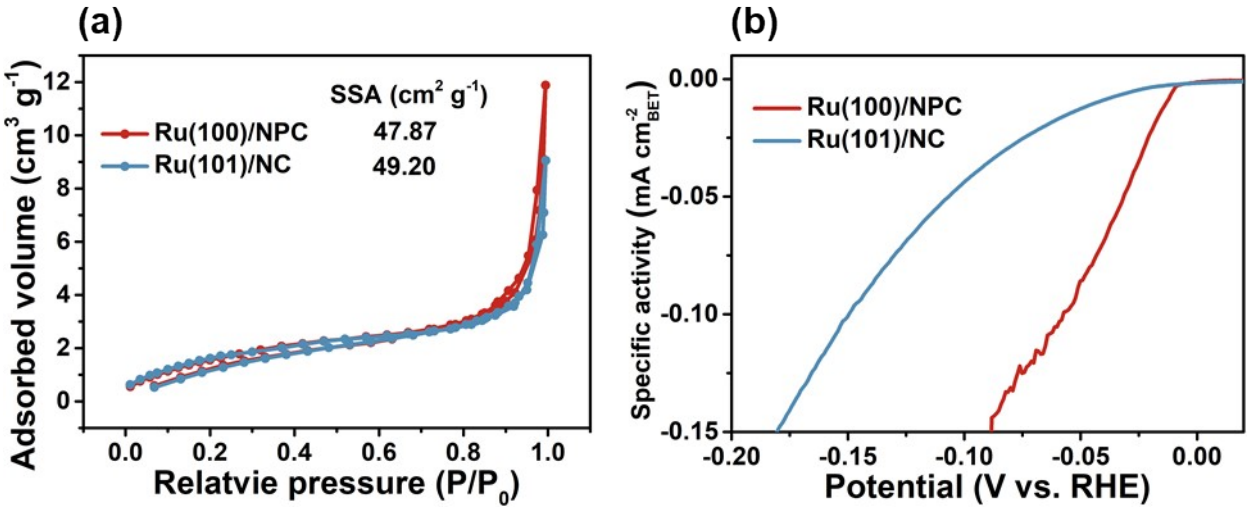

Fig. S11. (a) Nitrogen adsorption-desorption isotherm of Ru(100)/NPC and Ru(101)/NC. (b) Specific activity normalized to real surface area of Ru(100)/NPC and Ru(101)/NC as a function of applied potential.

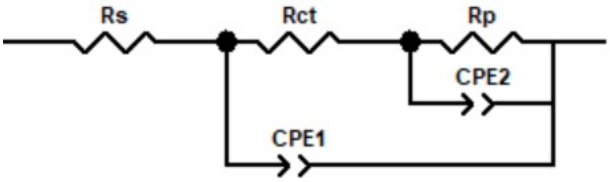

Fig. S12. The equivalent electric circuit.

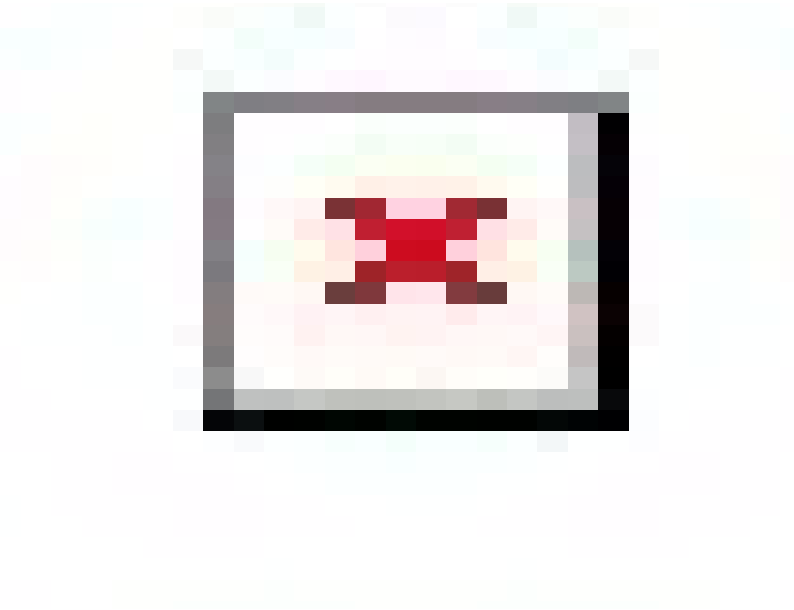

Fig. S13. The fitted data of R_p for Ru(100)/NPC.

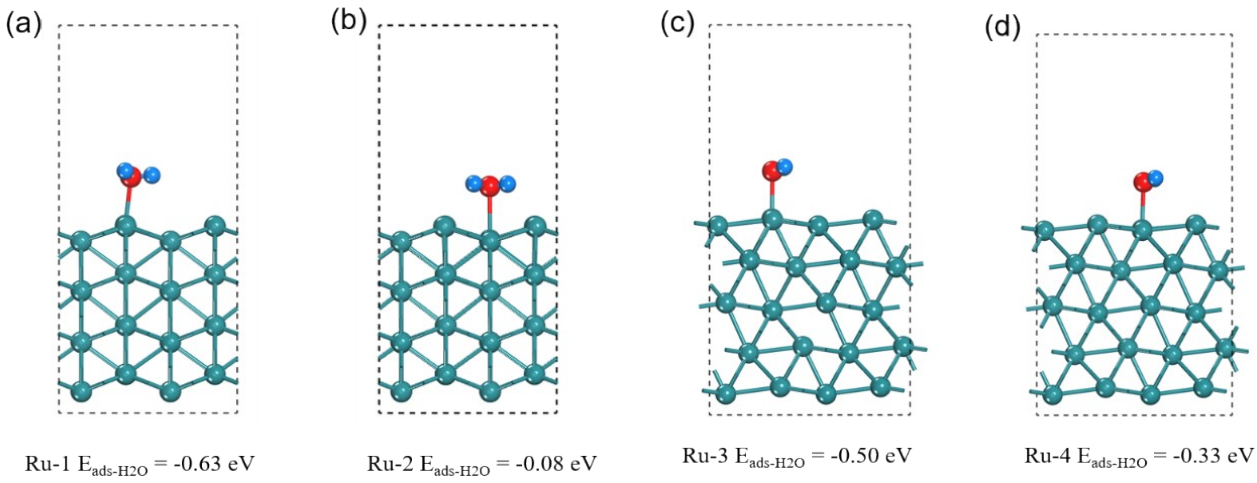

Fig. S14. The adsorption structures and adsorption energies at different sites.

Table S1. Comparison of the overpotential and corresponding Tafel slope with recently reported Pt-group based catalysts in alkaline conditions

	Electrocatalyst	Overpotential (mV)@10mAcm^{-2}	Tafel slope (mV dec^{-1})	Refs.
1	**Pt/C**	**37**	**29**	**This work**
2	**Ru(100)/NPC**	**16**	**19**	**This work**
3	IrGa/N-rGO	22	30.2	Adv. Energy Mater. 2022, 2202703
4	DSIrNi@CNTS	17	48	Adv. Mater. 2020, 32, 2006034
5	AC-Ir NSs	17	27	Nat. Commun. 2022, 13, 4200
6	IrMo/CNT	17	22	Nat. Commun. 2022, 13, 5497
7	IrRu DSACs	10	34	Angew. Chem. Int. Ed. 2023, 62, e202300873
8	RuAu SAA	24	37	Adv. Energy Mater. 2019, 9, 1803913
9	$RuRh_2$ bimetallene	24	31	Adv. Sci. 2021, 8, 2002341
10	RuNi/CQDs	13	40	Angew. Chem. Int. Ed. 2020, 59, 1718
11	RuBi SAA/Bi@OG	17.5	29.2	Angew. Chem. Int. Ed. 2023, 62, e202300879
12	RuNi NSs	15	28	Nano Energy 2019, 66, 104173
13	Pt SA-NiSe *V*	45	52	Angew. Chem. Int. Ed. 2023: e202308686
14	Pt/NiO_x-O_V	19.4	40.7	Adv. Funct. Mater. 2023, 33, 2211273
15	T-Pt-Co_4N	31	35	ACS Nano 2022, 16, 11, 18038-18047
16	PtC_{60}	24.3	41.9	Nat. Commun. 2023, 14, 1711
17	SLNP	14	30	Adv. Mater. 2020, 32, 1908521
18	Rh/MoOC	15	23.7	Small 2023, 19, 2206808

Table S2. Comparison of the mass activity with recently reported Ru-based electrocatalysts in alkaline media

	Electrocatalyst	Overpotential（mV）@10mAcm^{-2}	Tafel (mV dec^{-1})	Ref.
1	**$Ru_{0.85}Zn_{0.15}O_{2-\delta}$**	**50**	**1.998**	**This work**
2	**Commercial Pt/C**	**50**	**0.227**	**This work**
3	Ru@1T-MoS_2-MXene	100	0.79	Adv. Funct. Mater. 2023, 33, 2212514.
4	FeCoNiRu-450	100	1.307	Adv. Sci. 2023, 10, 2300094.
5	PdH_x@Ru	50	~0.28	J. Am. Chem. Soc. 2023, 145, 5710.
6	P,Mo-Ru@PC	25	1.525	Adv. Energy Mater. 2022, 16, 2200029.
7	Ru/Ni/WC@NPC	50	0.646	Adv. Energy Mater. 2022, 12, 2200332.
8	$Ni_{cluster}$-Ru NWs	50	1.417	Energy Environ. Sci. 2021, 14, 3194.
9	$RuRh_2$ bimetallene	50	1.49	Adv. Sci. 2021, 8, 2002341.
10	np-$Cu_{53}Ru_{47}$	50	0.199	ACS Energy Lett. 2020, 5, 192.
11	Ru/Ni_2P@NPC	100	1.567	ACS Sustainable Chem. Eng. 2019, 7, 17714.
12	Ru/$Y(OH)_3$ NHs	100	0.035	Chem. Commun. 2018, 54, 12202.
13	RuNC-2	100	0.87	Chem. Commun. 2018, 4, 13076.
14	Ru@GnP	25	0.23	Adv. Mater. 2018, 30, 1803676
15	$Cu_{2-x}S$@Ru NPs	100	0.098	Small 2017, 13, 1700052
16	1D-RuO_2-CN_x	100	0.05	ACS Appl. Mater. Interfaces 2016, 8, 28678.

References:

1 G. Kresse, J. Furthmüller, Efficient iterative schemes for ab initio total-energy calculations using a plane-wave basis set, *Phys. Rev. B,* 1996, **54**, 11169.

2 J. P. Perdew, K. Burke, M. Ernzerhof, Generalized gradient approximation made simple, *Phys. Rev. Lett.,* 1996, **77**, 3865.

3 G. Henkelman, H. Jónsson, Improved tangent estimate in the nudged elastic band method for finding minimum energy paths and saddle points, *J. Chem. Phys.,* 2000, **113**, 9978-85.

4 G. Henkelman, B.P. Uberuaga, H. Jónsson, A climbing image nudged elastic band method for finding saddle points and minimum energy paths, *J. Chem. Phys.,* 2000, **113**, 9901.

5 J.K. Nørskov, J. Rossmeisl, A. Logadottir, L. Lindqvist, J.R. Kitchin, T. Bligaard, H. Jonsson, Origin of the overpotential for oxygen reduction at a fuel-cell cathode, J. *Phys. Chem. B,* 2004, **108**, 17886.

6 C. Li, H. Jang, M. G. Kim, L. Hou, X. Liu, J. Cho, Ru-incorporated oxygen-vacancy-enriched MoO_2 electrocatalysts for hydrogen evolution reaction, *Appl. Catal. B,* 2022, **307**, 121204